RESEARCH AND APPLICATIONS IN STRUCTURAL DYNAMICS AND AEROELASTICITY

Irving Abel
NASA Langley Research Center
Hampton, Virginia

Introduction

Since the beginning of flight aeroelasticity and structural dynamics have played key roles in the design of almost every new airplane configuration. Engineers have continued to conduct tests and analyses to understand the physics of aeroelastic phenomena such as flutter, divergence, and buffet. In recent years the control of aeroelastic response has offered a potential for significant payoff in terms of aerodynamic efficiency and structural weight savings. Additionally, the advent of super computers has led to the development of computational unsteady aerodynamic algorithms that may lead to accurate prediction of aeroelastic response across the flight envelope. This fact will give the designer the ability to predict aeroelastic and dynamic response phenomena in the early stages instead of making costly fixes later based on flight test data.

As the "lead" NASA Center for airframe structures research a significant research program in aeroelasticity and structural dynamics is under way at the Langley Research Center. The technical objectives of this program include the demonstration of safety from aeroelastic instability for new aircraft configurations, the development of methods to control aeroelastic response, the development and verification of computational fluid dynamics methods applicable to unsteady air loads, and a fundamental understanding of the dynamic characteristics of new aerospace vehicles.

This paper presents the results of some selected studies in aeroelasticity and structural dynamics. This paper addresses research aimed at developing and validating control laws for the active control of aeroelastic response, at acquiring an experimental data base to validate new computational aeroelastic codes, at applying the latest state-of-the-art methodology to aircraft in hypersonic flight, at improving the aeroelastic response of aerospace vehicles through the use of adaptive materials, at developing new computational codes to predict unsteady aerodynamics, and at developing analysis and design methods to reduce rotorcraft vibrations.

Active Flexible Wing Program

The Active Flexible Wing (AFW) concept was developed by Rockwell International in the mid 1980's. The concept exploits wing flexibility to provide weight savings and improved performance. Weight savings is achieved by incorporating a very flexible wing with a configuration that requires no horizontal tail. In the wing design large amounts of aeroelastic twist are permitted to provide improved maneuvering capability at several design points. Since the configuration has no horizontal tail, the resulting degraded roll performance is overcome by the use of an active control system. The active control system uses multiple leading-edge and trailing-edge controls to provide acceptable roll performance up to and beyond control reversal. In addition, further weight reductions can be realized by using the active control system to provide flutter suppression, gust load alleviation, and maneuver load alleviation. It is estimated that an advanced fighter using this technology could achieve a 15 percent savings in takeoff gross weight.

The AFW active controls program, a joint effort of NASA Langley and Rockwell International, was an outgrowth of the AFW concept. A review of this program is presented in ref. 1. The goal was to demonstrate multi-input/multi-output multifunction digital control laws using a very sophisticated aeroelastic wind-tunnel model. Two wind-tunnel tests were conducted. The overall objectives of the program were to design the active control systems, to develop simulation techniques, and to demonstrate the designs during wind-tunnel tests. The control concepts that were evaluated were flutter suppression and rolling maneuver load control.

Wind-Tunnel Model

The AFW model mounted in the NASA Langley Transonic Dynamics Tunnel (TDT) is shown in Fig. 1. It is an aeroelastically scaled model of an advanced fighter aircraft. Two leading-edge and two trailing-edge control surfaces per wing panel were available to perform active control functions. The control surfaces were driven by miniature hydraulic actuators. The model was mounted on a sting that allowed the model freedom to roll about the sting axis. Figure 2 is a multiple-exposure photograph showing the model at four different roll angles. A brake was provided on the sting that allowed the model to be held in a fixed position when applied or allowed the model to roll when released. Model angle of attack could be changed remotely.

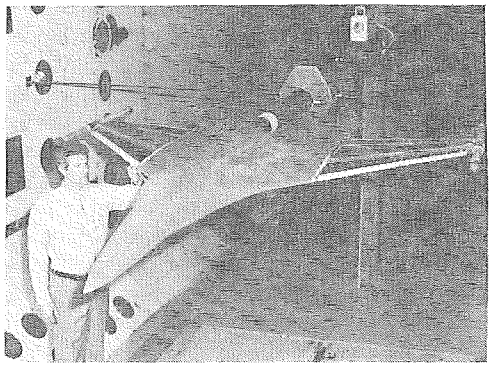

Figure 1. AFW model in the TDT test section.

In order for flutter to occur within the operating envelope of the tunnel, the model was tested with ballast tubes attached to each wing tip. The ballast tubes were designed to improve model safety when flutter occurs by employing a decoupler pylon mechanism.[2] When flutter is encountered, a latching mechanism is released from the ballast tube which decouples the ballast inertia from that of the wing resulting in a higher flutter velocity.

The digital controller used to implement the active control laws was specifically developed for this program.[3] It consisted of a SUN 3/160 Workstation modified to include

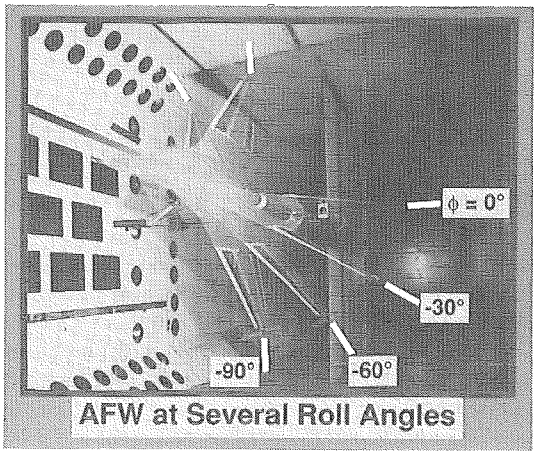

Figure 2. Multiple-exposure photograph of AFW model at four roll angles.

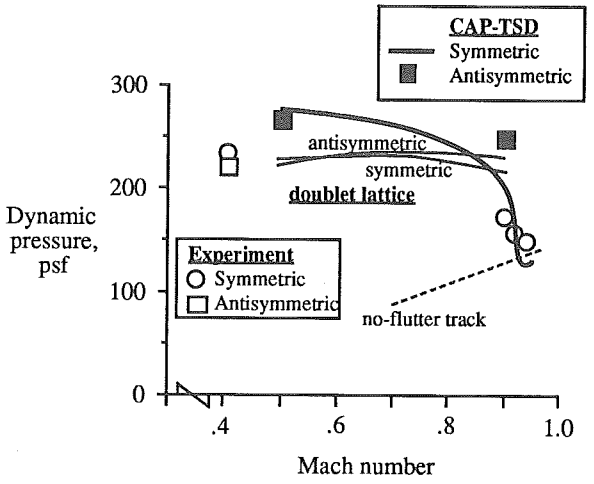

Figure 3. Comparison of calculated and measured flutter boundaries for the AFW model.

analog-to-digital and digital-to-analog conversion boards, digital signal processing boards, and a floating array-processing board. The digital controller provided sampling rates of 200 samples/sec. The controller could support the simultaneous operation of flutter suppression and rolling maneuver load control. In addition, the controller could record, transfer, and store digitized signals for data reduction.

Flutter Predictions

Subsonic flutter predictions were computed using a linear unsteady aerodynamic theory. Transonic flutter predictions were computed using the nonlinear Computational Aeroelasticity Program–Transonic Small Disturbance (CAP-TSD) code.[4] A description of the nonlinear analysis method applied to the AFW configuration is given in ref. 5. Mode shapes, frequencies, and generalized masses for the first ten symmetric and antisymmetric elastic modes were used to form the equations of motion. Linear flutter predictions using doublet lattice unsteady aerodynamics for symmetric and antisymmetric motions, with the model fixed-in-roll, are shown in Fig. 3. When the model is fixed-in-roll both symmetric and antisymmetric flutter occurs within the tunnel operating envelope. When the model is free-to-roll the antisymmetric flutter boundary moves outside the tunnel envelope. Also shown is a nonlinear CAP-TSD computation of the symmetric flutter boundary. Experimental results obtained from the tunnel tests are also presented. Linear theory adequately predicts the flutter boundary at subsonic speeds, but it fails, as expected, to predict the very sudden drop in stability observed at transonic speeds. Conversely, the CAP-TSD computation predicts a very severe transonic flutter "dip" but overpredicts the flutter dynamic pressure at subsonic speeds. Studies are continuing to correct the modeling in an attempt to improve correlations across the Mach number range.

Control Law Design

Both flutter suppression and rolling maneuver control laws were synthesized, implemented, and tested on the AFW model. The first objective of the testing was to demonstrate flutter suppression. Due to the proximity of the symmetric and antisymmetric flutter boundaries to one another for the model fixed-in-roll, for any substantial increase in flutter speed the flutter suppression system has to suppress both flutter modes simultaneously. The second objective was to demonstrate the simultaneous operation of multiple control functions. In this case, with the model free-to-roll, the objective was to demonstrate the simultaneous operation of symmetric flutter suppression and rolling maneuver control.

A block diagram of the flutter suppression system is shown in Fig. 4. Sensor signals, in the form of accelerometer outputs, from each wing are summed and differenced to form symmetric and antisymmetric signals. These signals are then processed by their respective control laws. The processed signals are recombined to form the appropriate actuator commands. Three flutter suppression control designs were synthesized and implemented at NASA Langley. Table 1 contains a summary of the control surfaces and sensor locations used by each control law. The methodology used to synthesize the three control laws included a reduced-order LQG[6] method (FSS 1), a traditional pole/zero placement[7] method (FSS 2), and a multi-input/multi-output constrained optimization[8] method (FSS 3).

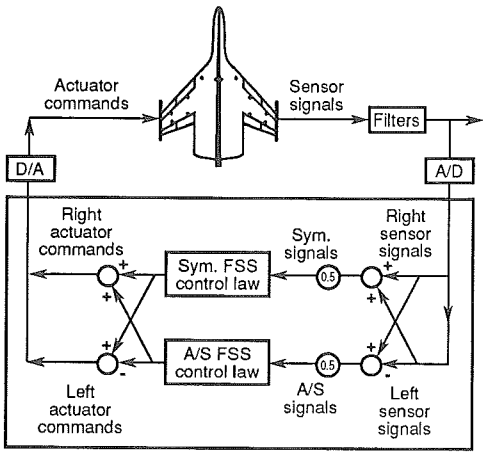

Figure 4. Flutter suppression block diagram.

Table 1. Flutter suppression control law description.

Synthesis Methods	Symmetric Controls/ Sensors	Symmetric Control Law Order	Antisymmetric Controls/ Sensors	Antisymmetric Control Law Order
FSS 1	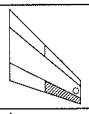	5th	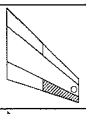	5th
FSS 2	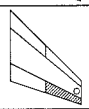	3rd	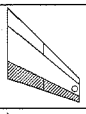	3rd
FSS 3	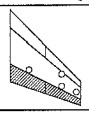	11th	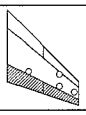	8th

° Accelerometer

The design objective of the rolling maneuver control laws was to reduce or limit wing loads during rolling maneuvers of 90 degrees. Two roll control concepts (Rolling Maneuver Load Alleviation–RMLA[9] and a Roll Rate Tracking System–RRTS[10]) were evaluated. The objective of the RMLA was to reduce the incremental bending and torsion moments acting on the model while trying to maintain a constant roll performance. The objective of the RRTS was to limit the total loads while maintaining constant roll performance. Both control laws were designed to operate, with the model free-to-roll, at tunnel conditions above and below the passive flutter boundary.

Test Results

Open-loop flutter results were needed to assess the performance of the active control systems in suppressing flutter. Experimental flutter results are shown in Fig. 3. Open-loop results were acquired at subsonic and transonic speeds. Due to operating limitations on the tunnel during these tests only subsonic closed-loop results were acquired.

Flutter suppression tests were conducted on the fixed-in-roll and the free-to-roll configurations. All closed-loop flutter suppression testing was performed at Mach numbers between $M = 0.4$ and $M = 0.5$. Experimental results (Fig. 3) indicate that the symmetric and antisymmetric flutter modes for the fixed-in-role configuration are very closed to one another at subsonic speeds. To suppress flutter for this configuration the control law must suppress both modes simultaneously. All three flutter suppression systems were tested for this configuration. The results are presented in Fig. 5. As shown, the control laws for the fixed-in-roll configuration suppressed both symmetric and antisymmetric flutter modes at dynamic pressures up to 26 percent above the antisymmetric open-loop boundary and up to 17 percent above the symmetric open-loop boundary. Closed-loop flutter was not encountered but testing was limited to the dynamic pressures indicated in the figure due to high dynamic response of the wing for all the control laws. In similar tests for the free-to-roll configuration all control laws demonstrated 23 percent increases in dynamic pressures over the symmetric open-loop boundary. Closed-loop flutter was not encountered, but testing was terminated because the tunnel operating limits were reached.

A typical RMLA result is presented in Fig. 6. The dashed line in the figure represents a baseline roll maneuver for compression purposes. The solid line RMLA maneuver shows a nearly identical roll maneuver but with significantly different incremental outboard torsion moment time histories. The RMLA reduced the peak load by more than 50 percent. The control law utilized the trailing-edge inboard and the leading-edge outboard control surfaces. The data shown were measured at $M = 0.4$ and a dynamic pressure of 200 psf. A more complete description of the RMLA testing can be found in ref. 9.

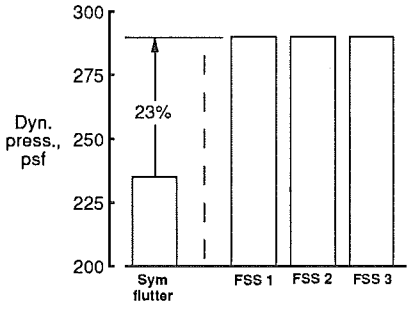

(a) Free-to-roll flutter suppression.

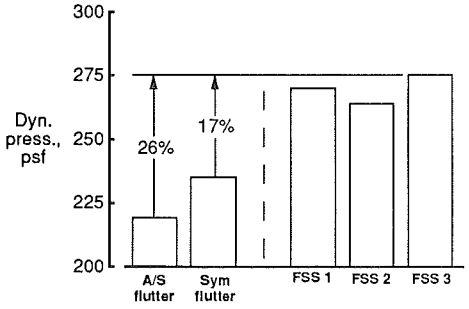

(b) Fixed-in-roll flutter suppression.

Figure 5. Flutter-suppression results.

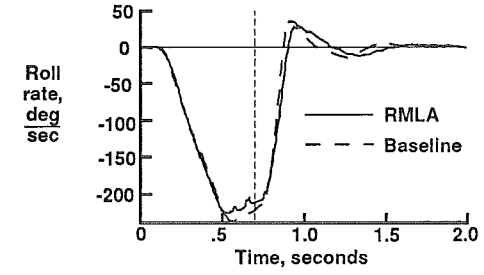

(a) Roll rate comparison

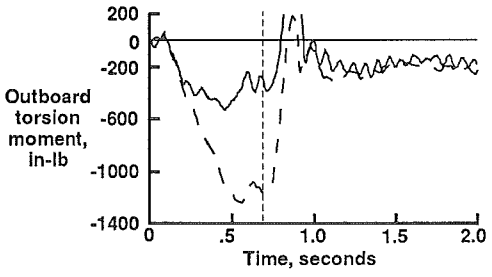

(b) Torsion moment comparison

Figure 6. Typical RMLA performance.

A typical RRTS result is presented in Fig. 7. In the maneuver presented the model was rolled 90 degrees in .48 sec. at $M = 0.4$ and a dynamic pressure of 250 psf. The RRTS system only controls loads when they exceed some specified level. The roll-rate time history is shown along with the measured inboard torsion moment. The torsion moment was kept below 1800 in. lbs. in the example shown. A more complete description of the RRTS testing can be found in ref. 10. Both control laws were tested in combination with flutter suppression above the symmetric open-loop flutter boundary demonstrating multifunction operation.

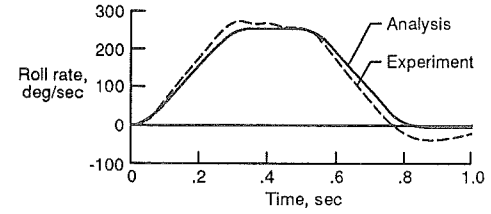

(a) Roll rate comparison

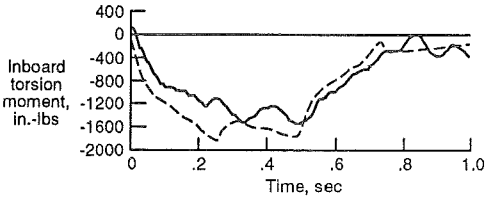

(b) Torsion moment comparison

Figure 7. Typical RRTS performance.

Benchmark Models Program

A significant number of aeroelastic problems can occur at transonic speeds including the minimum flutter speed, buffeting, control surface buzz and other non-classical instabilities such as shock-induced limit-cycle oscillations. Computational Fluid Dynamic (CFD) codes currently hold promise for being able to analytically predict these phenomena. However, the assessment of these codes is far from complete. For example, much flutter data are available in the literature but most of the data are not suitable for code validation purposes because of missing details in the documentation. To fill this void, an experimental program called the "Benchmark Models" program has been developed at NASA Langley. The primary purpose of the program is to provide well documented experimental data that can be used to validate computational codes. In addition, the data will be used to understand the physics of unsteady flows and can be used to provide data for empirical design purposes. Experimental data sets will include a complete description of the model geometry; a complete definition of the structural dynamic characteristics including modal frequencies, dampings, generalized masses, and mode shapes; measured flutter boundaries including flutter velocity, frequency and mode shape; measured unsteady pressures acquired during flutter on at least two chords; a qualitative indication of transition and flow separation; and flow visualization where possible

Program Overview

The Benchmark Models Program[11] is a multi-year program. Tests are to be performed in the TDT at a rate of approximately two tests per year. The plan is to begin with simple rigid models on a flexible mount system and then to move to more complex flexible models.

Initial tests have been performed on the Pitch and Plunge Apparatus[12] (PAPA) using rigid models. The PAPA is a mount system specifically designed for this type of testing. A photograph of the mount system in the TDT is shown in Fig. 8. The mount system consists primarily of four steel rods that attach at one end to a turntable on the tunnel wall and at the other end to a moving plate in the test section where the model is mounted. The four rods permit both plunge and torsional degrees of freedom and also provide linear plunge and pitch stiffnesses for elastic restraint. A thin central beam stiffens the mount system in the fore and aft direction. The turntable permits the angle of attack to be changed remotely. The wing root of the model is attached to the moving plate. A photograph of the entire mechanism including the model and splitter plate installation is shown in Fig. 9. The PAPA is instrumented to provide instantaneous measurements of plunge position and pitch angle. The aeroelastic system

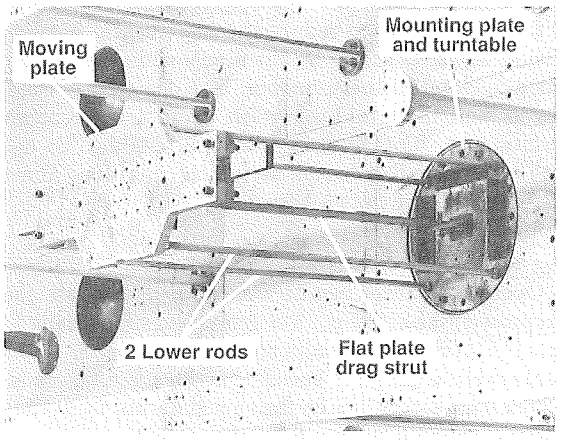

Figure 8. PAPA flexible mount.

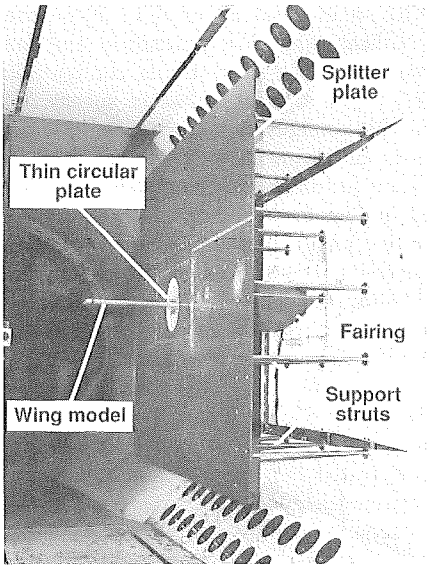

Figure 9. Complete PAPA system.

is comprised of a rigid airfoil attached to a flexible mount. The structural properties of the mount system are well defined and documented. The PAPA system is quite rugged and robust thus permitting the measurement of multiple flutter points with little risk to the model or mount system.

Wind-Tunnel Models

The initial wing tested in the program is shown mounted in the tunnel in Fig. 10. Currently there are three rigid models with different airfoil sections in this series of tests. The three airfoil sections are a NACA 0012 airfoil, a NASA supercritical airfoil SC(2)-0414, and a NACA 64A010 airfoil. The three airfoils have been selected because of their varying types of transonic flow development.

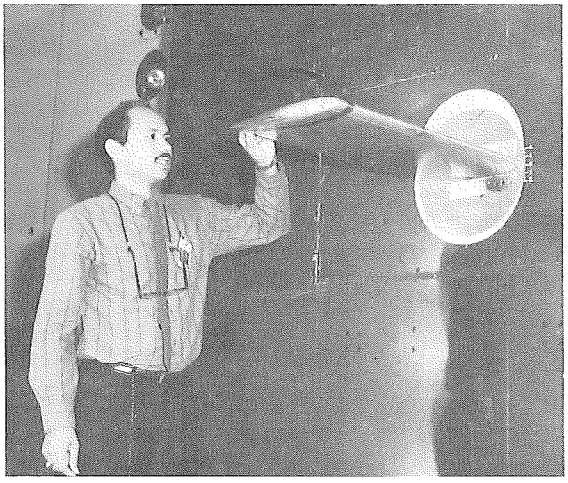

Figure 10. NACA 0012 airfoil model mounted in TDT.

All PAPA models in this series of tests are rectangular in planform. As shown in Fig. 11, they have a 16 in. chord and a semispan of 32 in. All three models have two rows of in-situ pressure tranducers, one row is located at 60 percent span and the other row at 95 percent span. Each row contains 40 unsteady pressure transducers. The models are machined from aluminum. In addition to pressure transducers, accelerometers are installed near the four corners of the wing. Details of the construction of the NACA 0012 airfoil are shown in Fig. 12.

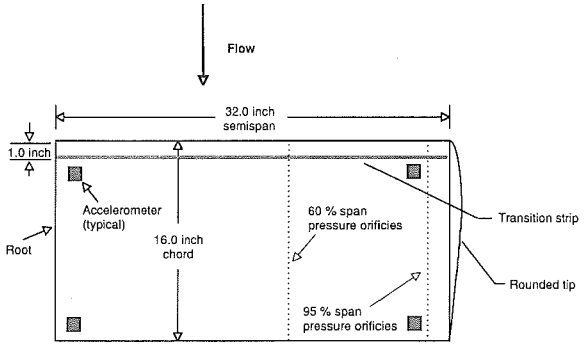

Figure 11. Wing model planform.

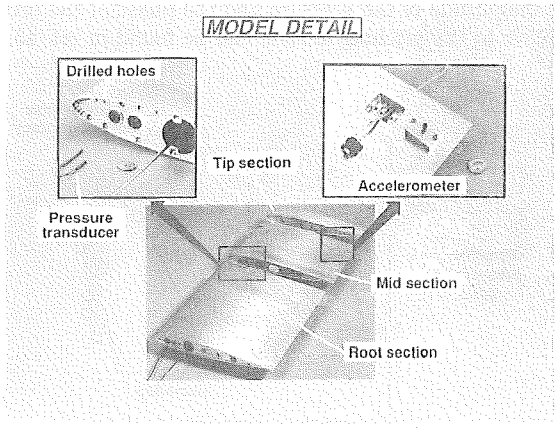

Figure 12. Model details.

Following the three airfoil section tests, an active controls model will be fabricated and tested. This model will be similar to the NACA 0012 model but in addition will have a movable trailing-edge control surface at the 30 percent span station with a chord length of 25 percent of the wing chord. Upper and lower surface wing spoilers with a chord length of 15 percent of the wing chord will be located in line with the trailing-edge control. Unsteady pressure measurements will include areas near the hinge lines of the control surface and the spoilers. The model will be mounted on a five component balance to acquire static and dynamic loads on the model produced by actuating the control surface and spoilers. Various control laws will be designed and implemented on the model.

Results of Initial NACA 0012 Model Tests

Conventional flutter, plunge instability, and stall flutter boundaries measured as a function of dynamic pressure versus Mach number for the NACA 0012 model are presented in Fig. 13. The conventional flutter boundary at zero degrees angle of attack (Fig. 13a) is well defined. A small transonic dip is apparent at $M = 0.77$ followed by a sharp upturn of the boundary near $M = 0.80$. Over a narrow Mach number range between $M = 0.88$ and $M = 0.95$ a flutter motion consisting primarily of a plunging motion was also identified. Flow visualization in this region indicated strong shock-induced separation in this Mach number region. At $M = 0.78$ the flutter boundary as a function of angle of attack was measured (Fig. 13b). As shown, flutter dynamic pressure increases slightly until about 4 degrees where there is a rapid decrease in flutter dynamic pressure which is associated with wing stall during a portion of the pitch cycle.

Wing surface pressure measurements were acquired at most of the flutter points. An example mean pressure plot at transonic speeds during conventional flutter is shown in Fig. 14. Plotted are the mean values of pressure coefficient C_p of the upper surface during flutter as a function of chord position at the 60 and 95 percent span stations. The data presented are for $M = 0.77$, 0.80, and 0.82. For the 60 percent span station data, it can be seen that the shock strengthens and moves aft to near the 40 percent chord station as M increases from 0.77 to 0.82. At the 95 percent span station a weak shock appears near the 20 percent chord station at $M = 0.80$ and 0.82. Other test results including

the magnitude of the pressure and the phase of the pressure relative to the pitching motion can be found in ref. 13.

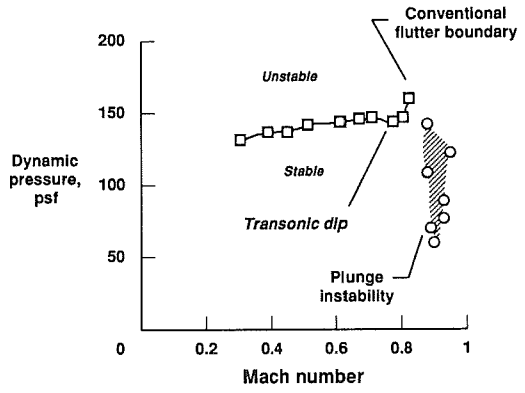

a. Conventional flutter boundary and plunge instability region (angle of attack = 0 degrees).

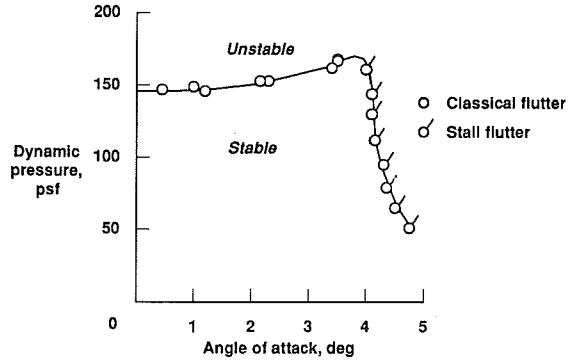

b. Stall flutter boundary versus angle of attack at $M = 0.78$.

Figure 13. NACA 0012 flutter boundaries.

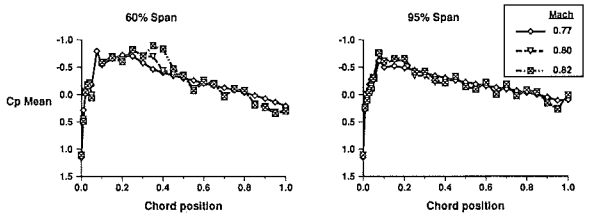

Figure 14. Upper surface mean pressure coefficient during conventional flutter for several Mach numbers.

Hypersonic Aeroservothermoelasticity

Significant aerothermal loads are generated on vehicles which travel through the atmosphere at high supersonic and hypersonic speeds. These aerothermal loads alter the flexibility of the vehicle through changes in the material properties and through thermal gradients which change the stress levels. Changes in the flexibility of the structure can significantly alter the aeroelastic response of the vehicle.

An analytical study[14] was conducted to predict the aeroelastic response characteristics of an aerodynamically heated generic hypersonic vehicle and to design an active control system to alleviate any adverse effects caused by heating. The generic hypersonic vehicle configuration is shown in Fig. 15. First, the steady-state aerodynamic forces and heat loads were determined for the chosen flight conditions using a state-of-the art analysis package. These heat loads were then used to determine the changes in material properties and structural stiffness. A comparison of natural frequencies for the first six symmetric structural modes between the "hot" and "cold" conditions is given in Table 2. When the effects of heating are included the natural frequencies drop by 13 to 20 percent. However, the effect on the mode shapes was small.

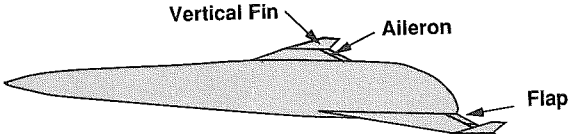

Figure 15. Generic hypersonic vehicle.

Table 2. Vibration mode descriptions and natural frequencies.

MODE	DESCRIPTION	FREQUENCY (HZ)		% REDUCTION
		COLD	HOT	(COLD-HOT / COLD)
1	fuselage bending	3.01	2.43	19.3
2	wing bending	4.02	3.48	13.4
3	second fuselage bending	7.06	5.67	19.7
4	wing torsion	7.70	6.56	14.8
5	all-movable fin mode	9.47	7.63	19.4
6	highly coupled mode	10.96	8.84	19.3

The finite-element model of the heated structure was used to assess the effects of heating on flutter and on the short period dynamics. Figure 16 shows the effect of heating on the flutter dynamic pressure q_f at $M = 2$ and $M = 4$. Reductions in flutter dynamic pressure from the cold condition of approximately 45 percent at $M = 2$ and $M = 4$ are shown. The results presented in ref. 14 also indicate that including the heating has a destabilizing effect on the short period mode.

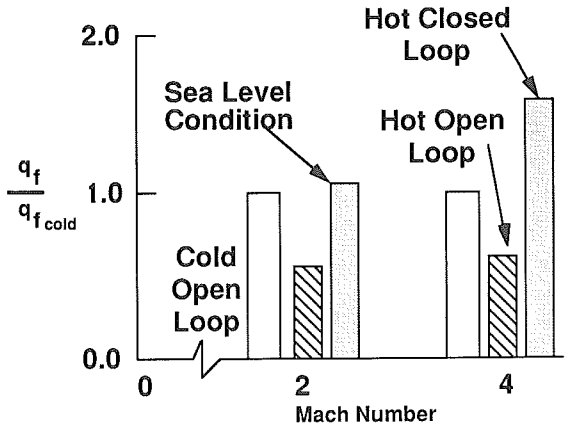

Figure 16. Flutter results.

Due to the large degradation in the flutter characteristics of the vehicle the use of a flutter suppression system was investigated. For the flutter suppression system design, a full-order state estimater (Kalman Filter) was used for compensation. The controller was designed using standard Linear Quadratic Gaussian methods. Normal acceleration at the pilot station and at a location near the wing aileron were used for feedback. The aileron and flap were used as active controls. The results in Fig. 16 show that the active control system can increase the flutter dynamic pressure far beyond that of the "cold" vehicle. At $M = 2.0$ the FS system stabilized the vehicle for all conditions above sea level.

In an attempt to reduce accelerations at the pilot station a ride quality augmentation system (RQAS) was also designed. The purpose was to evaluate the potential for reducing turbulence induced accelerations felt by the pilot due to excessive fuselage flexibility. The controller was designed using an eigenvalue assignment technique. The same sensors were used in the RQAS that were used in the flutter suppression system. The flap was used as the feedback control surface because it has much more influence on pilot station response than the aileron. Control surface displacements were limited to 10 degrees and rates were limited to 30 degrees per second. The performance of the RQAS can be asessed by comparing the open-loop and closed-loop power spectral densities in Fig. 17 of vertical accelerations at the pilot station $\Phi\ddot{z}(\omega)$ for the "hot" vehicle encountering a 1 foot-per-second gust. The RQAS reduces the peak acceleration at the pilot station by 54 percent.

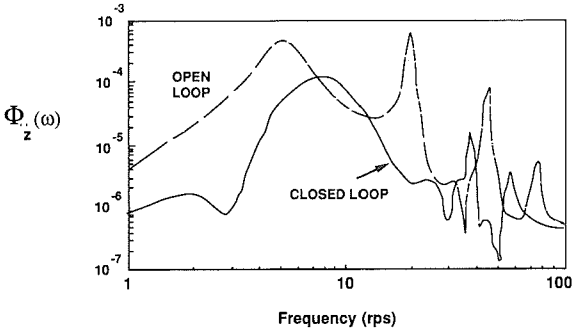

Figure 17. Ride quality results.

The results of this study indicated that for a hypersonic vehicle aerodynamic heating can significantly affect the aeroelastic characteristics. In addition, active controls can be used effectively to improve the "hot" aeroelastic characteristics of such vehicles.

Flutter Suppression Using Piezoelectric Materials

The use of adaptive materials to control aeroelastic response is receiving significant attention. Static aeroelastic control of composite wings with embedded actuators is described in refs. 15 and 16. Reference 17 analytically investigated the use of adaptive materials to control flutter. A recent experimental study[18] validated the use of piezoelectric materials to control flutter.

For the study in ref. 18 a two degree-of-freedom model was designed and tested in a small table top wind tunnel. The model consisted of a rigid airfoil attached to a flexible mount system. The wind tunnel has a top speed of about 85 mph. The test section is 6 in. square. The wing core is constructed of a solid aluminum plate with balsa wood providing the aerodynamic contour. The mount system permits pitch and plunge degrees of freedom. Plunge and pitch stiffnesses are provided by steel springs. Peizoelectric actuators were installed near the root of one of the bending springs of the mount system. Strain gauges were also mounted on the springs to measure bending strain and these signals were used as feedback for the controller. A sketch of the wind tunnel along with a photograph of the test section and model is shown in Fig. 18.

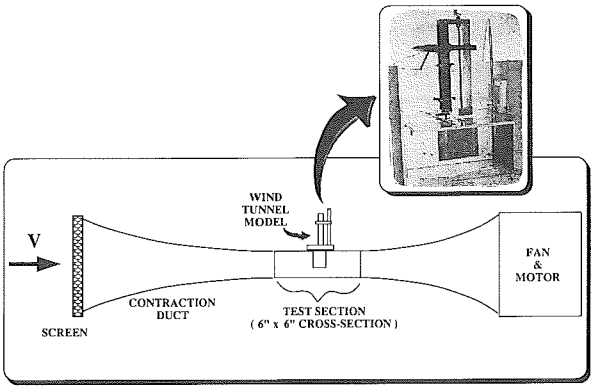

Figure 18. Wind tunnel and model.

A finite-element model of the wing and mount system was developed. The purpose of the analytical model was to generate mass and stiffness matrices so that the wind-tunnel model could be mass balanced to flutter in the tunnel and for analyzing the performance of different control laws. Unsteady aerodynamics were generated using a classical doublet-lattice method. A comparison of the flutter speed between analysis and experiment for the wind-tunnel model is shown in Fig. 19. The experimental flutter speed was determined by increasing the tunnel fan speed until model oscillations remained sinusoidal. Tunnel turbulence was used to perturb the model motion. As shown in Fig. 19, the open-loop analysis is slightly conservative in predicting the open-loop flutter speed.

A simple single-input single-output gain feedback flutter suppression control law was designed using traditional gain root locus methods. The control law was implemented using a personal computer operating in a real time Unix environment. Command signals, in terms of applied voltages, generated by the computer were applied to the piezoelectric actuators thereby modifying the bending stiffness properties of the leaf springs.

A comparison of closed-loop flutter speed between analysis and experiment is also presented in Fig. 19. As was the case for the open-loop results, the analysis is slightly conservative in predicting the closed-loop flutter speed. It should be noted that the flutter speed increase was predicted to be improved by about 16 percent but in actuality the controller improved the flutter speed by 20 percent. A comparison of open-loop and closed-loop dynamic response is presented in Fig. 20. Shown in the figure is a comparison of strain guage response due to wind-tunnel turbulence for the open-loop and closed-loop systems just below the open-loop flutter

speed. As would be expected significant differences between the open-loop and closed-loop systems are evident. This research effort represents the first documented evidence that adaptive materials can be used to suppress flutter. Future studies will evaluate their use to control buffet response, gust response, and maneuver loads.

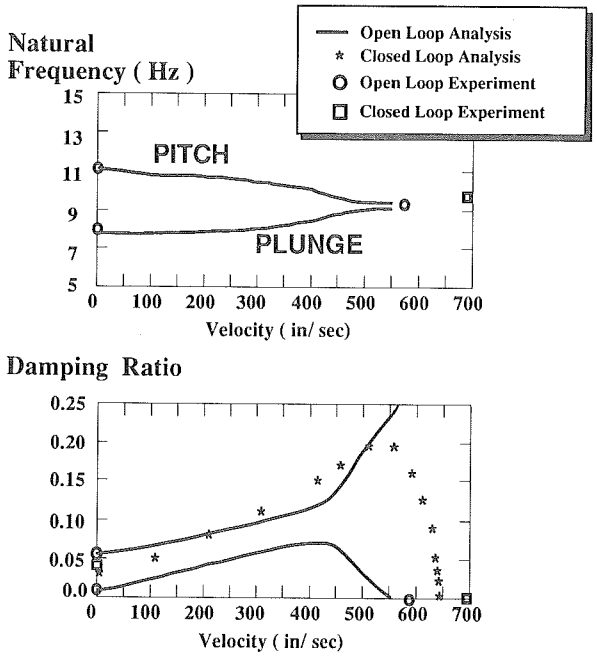

Figure 19. Analytical and experimental flutter results.

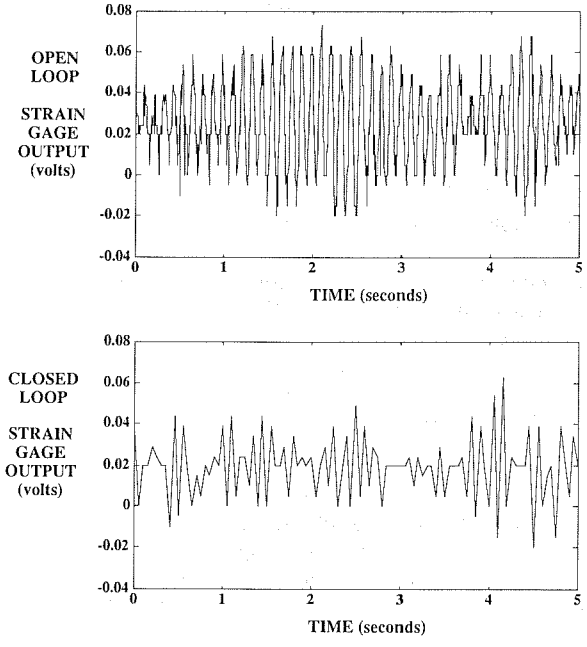

Figure 20. Experimental open-loop and closed-loop strain response to wind-tunnel turbulence just below flutter velocity.

Unstructed-Grid Methods Development for Aeroelastic Analysis

Over the last two decades there has been significant progress in developing computational fluid dynamics (CFD) methods for aerodynamics analysis. Reference 19 presents a review of CFD methods for transonic unsteady aerodynamics and their use for aeroelastic applications. The necessity to accurately establish the aeroelastic characteristics of a vehicle are crucial since the occurrence of flutter within the flight envelope often leads to structural failure and loss of the vehicle. In addition, the service life of a vehicle can be altered significantly by unforeseen dynamics loadings, such as buffet or gust response. The ability to accurately predict such aeroelastic phenomena across the Mach number range is of great importance to achieving a problem free final design. Advances in unsteady CFD methods have paralleled those in steady CFD methods developed but with a substantial time lag due to the added complexity of requiring time accuracy. Grid generation for aeroelastic analysis where the mesh moves to conform to the instantaneous position of the deforming flexible vehicle, which is required for calculations using Euler and Navier Stokes algorithms, significantly increases the complexity and cost of aeroelastic calculations.

Two competing schemes that are used to obtain the grid layouts needed for CFD problems are the structured and unstructured grid methods. Unstructured grids have several advantages over structured grids for aeroelastic calculations. The first is the ability of unstructured grids to easily model very complicated three-dimensional geometries such as the 747 transport shown in Fig. 21. The 747 geometry includes

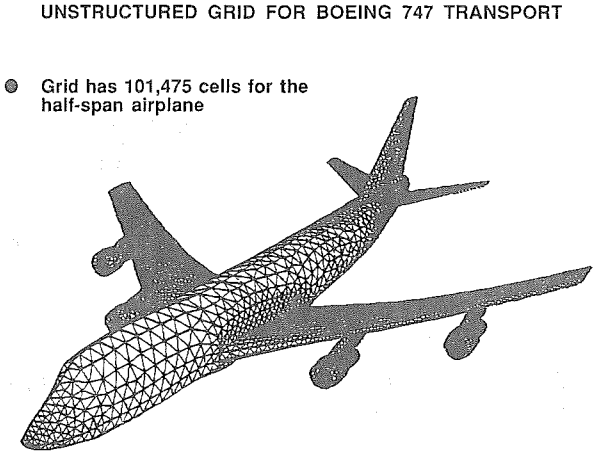

Figure 21. Surface mesh of triangles for the Boeing 747 aircraft.

the fuselage, the wing, the vertical and horizontal tails, the underwing pylons, and the flow through nacelles. The unstructured mesh contains 101,475 tetrahedrans and 19,055 nodes for symmetric analysis wherein it is only necessary to model one-half the airplane. With a structured grid it is very difficult to achieve this level of geometric complexity. Another advantage of unstructured grids is that the methodology permits the structural deformations of the vehicle to be treated in a general way. An example of a deforming surface grid for a supersonic fighter configuration oscillating in a vehicle bending mode is shown in Fig. 22. The bending

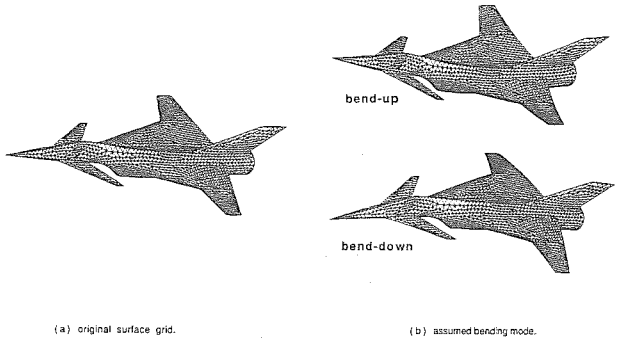

Figure 22. Surface grid for deforming supersonic fighter configuration.

mode is exaggerated by a factor of five. The deforming grid capability does not involve any assumptions which limits its applications to small deformations. Reference 20 presents a method for moving body conforming meshes during aeroelastic motions. The method relies on a spring analogy where the length of a mesh cell edge is related to the stiffness of a spring. A third advantage of unstructured grids is that they enable a natural way to use adaptive mesh refinement based on flow physics. For example, Fig. 23 shows a conical vortex dominated flow solution for a flat plate delta wing at $M = 1.4$, an angle of attack α of 20 degrees, and a sideslip angle β of 10 degrees. The solution was obtained by adapting the original mesh three times to the instantaneous flow. The final result shown in Fig. 23 is a highly accurate solution of the conical Euler equations produced by an unstructured grid of 3261 nodes with an order of magnitude less grid points than is required for a structured grid to obtain equivalent results.

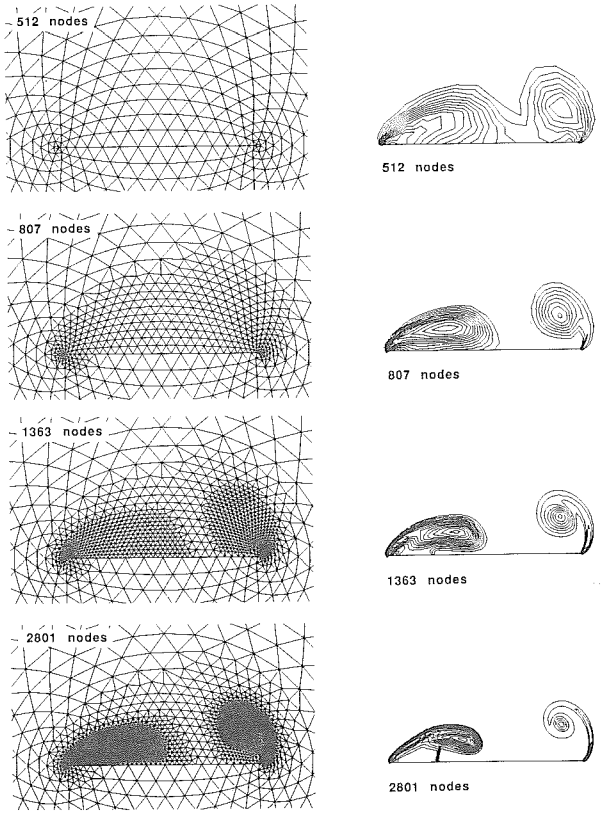

Figure 23. Effects of adaptive mesh refinement on the total pressure loss contours for a 75 degree swept flat-plate delta wing computed using conical Euler equations at $M = 1.4, \alpha = 20$ degrees, and $\beta = 10$ degrees.

An example of a CFD calculation using a central-difference-type Euler solver[20] for the supersonic fighter mentioned above is presented in Fig. 24. The results were calculated using a grid of 13,832 nodes and 70,125 tetrahedra. Instantaneous pressure distributions on the surface of the vehicle at maximum amplitudes of bend-up and bend-down for two angles of attack are shown in the figure. The Mach number was 2.0 and the reduced frequency k, based on wing tip semi-chord, was 0.1. These results indicate the ability of unstructured grids to treat complex configurations.

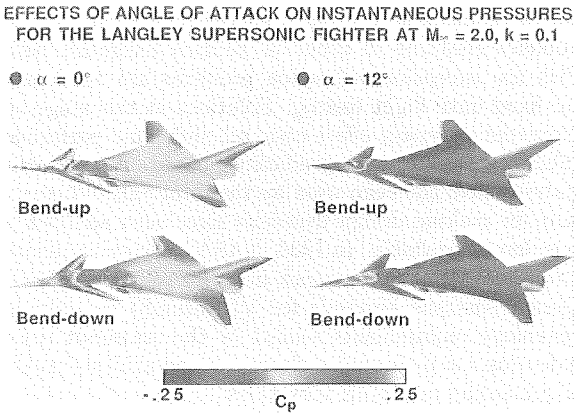

Figure 24. Effects of angle of attack on the instantaneous pressure coefficient contours of a supersonic fighter configuration at the maximum (bend-up) and minimum (bend-down) amplitudes of deformation computed using an Euler flow solver at $M = 2.0$ and $k = 0.1$.

A demonstration of spatial adaption procedures is presented in ref. 21 for a NACA 0012 airfoil pitching sinusoidally about its quarter chord. The freestream Mach number was 0.755, the pitching amplitude was 2.51 degrees, and the reduced frequency k (based on semi-chord) was 0.08. Some results from this study are presented here in Fig. 25 as the instantaneous spatially adapted meshes for eight points during the pitching oscillation cycle. In each plot, the instantaneous pitch angle $\alpha(\tau)$ and the instantaneous angular position $k\tau$ is shown. The grid was modified based on the substantial derivative of the density which includes both spatial and time variations. The mesh was enriched in regions of high gradients and coarsened where points were not needed, allowing solutions of high spatial accuracy to be produced at minimal computational cost. The instantaneous meshes shown in Fig. 25 clearly indicate that the mesh is enriched in regions near the shock waves and at the stagnation points. The advantage in the adaptation procedure is that the mesh geometry is driven by the physics of the problem.

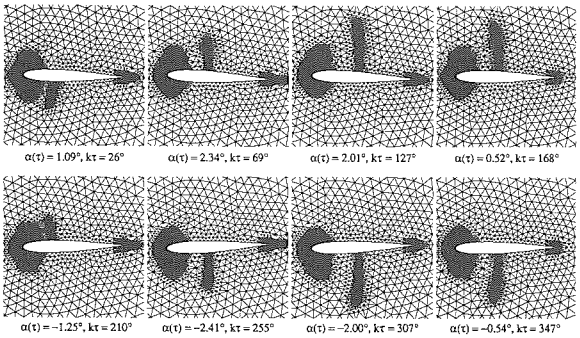

Figure 25. Instantaneous meshes produced by the spatial adaption procedure for an NACA 0012 airfoil pitching harmonically at $M = 0.755$, and $k = 0.0814$.

Rotorcraft Structural Dynamics

Excessive vibrations have plagued the development of most new rotorcraft. Although vibration levels have been reduced considerably in each successive aircraft, vibration problems continue to occur in modern rotorcraft designs. With few exceptions vibration problems are not identified and fixed until flight testing. Solutions at this stage of development adversely effect cost, schedule, and performance. Until recently vibration predictions based on finite-element analyses have not been used by the rotorcraft industry as a basis for making design decisions since such analyses were considered unreliable. In 1984, NASA Langley implemented a program with the rotorcraft industry called "DAMVIBS" (Design Analysis Methods for VIBrationS) to address the technology requirements needed by the rotorcraft industry to develop a superior finite-element based analysis capability for predicting rotorcraft vibrations.

The problems facing the rotorcraft dynamicist are formidable as depicted in Fig. 26. The rotor system itself transmits complex periodic loads to the airframe both aerodynamically through the wake and mechanically through the mounting system. The airframe structural dynamics problem is further complicated by the fact that helicopter airframes are usually lightweight, shell-type structures having multiple large cutouts. A major deficiency has been an incomplete understanding of the finite-element modeling requirements as they apply to helicopters. The scope of the DAMVIBS program included finite-element modeling, difficult components studies, coupled rotor-airframe vibrations, and airframe structural optimization. The primary emphasis was on finite-element modeling and the difficult components studies.

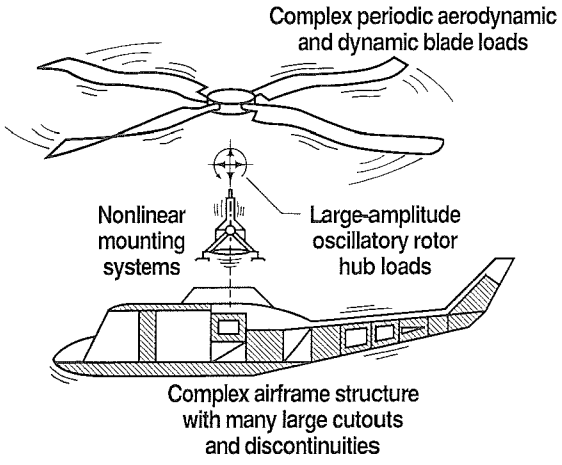

Figure 26. Challenges confronting analysts in predicting helicopter vibrations.

The purpose of the airframe finite-element modeling element was to develop state-of-the-art finite-element models for internal loads and vibration analysis of airframes constructed of both metal and composite materials. Industry teams from Bell Helicopter Textron, Boeing Helicopter, McDonnell Douglas Helicopter, and Sikorsky Aircraft formed finite-element models, conducted ground vibration tests, and made extensive comparisons of results of the vehicles shown in Fig. 27. Ground vibration test aircraft are shown in Figs. 28, and typical comparisons of tests and analyses are shown in Fig. 29. The general conclusions drawn by the work in finite-element modeling indicated that: up-front planning is required before modeling begins; all groups including statics, dynamics, and weights must work closely together; modeling techniques for metal and composite structures are similar except for the determination of material properties; a better definition and representation of damping is required; and comparisons between analytical and experimental vibration results are in good agreement through about 10 Hz, partially satisfactory between 10 and 20 Hz, and generally unsatisfactory above 20 Hz.

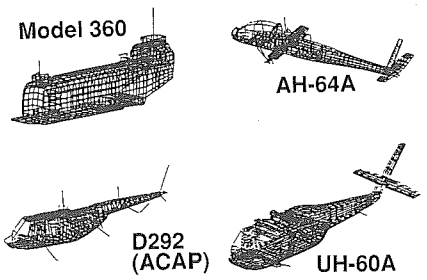

Figure 27. Finite element models formed.

The purpose of the difficult components studies was to identify the effects of representing nonprimary structure as lumped masses and to develop improved modeling guides for secondary structures. A difficult components study was conducted on the Bell AH-1G helicopter shown in Fig. 30. The aircraft fully assembled is shown in Fig. 30a. Components were then progressively removed starting with the main rotor and transmission assembly, secondary structural panels, tail rotor drive shaft, skid landing gear, and engine. The resulting stripped-down configuration is shown in Fig. 30b. Later, the stub wings and canopy were removed in the last step. At each step an analysis based on a finite-element model of the existing structure was compared with ground vibration tests. Comparisons were used to identify components which were causing errors, and the modeling of these components was improved. Based on these results an updated finite-element model was generated to include components which had not been modeled properly. The improvement in predictive capability is shown in Fig. 31. It can be seen

that calculations of natural frequencies using the updated finite-element model are generally within 5 percent of the experimental data as compared to 20 percent using the original model. The general conclusions drawn from this study are: the stiffness of tight secondary structural panels and canopy glass are important and must be modeled in detail; lumped mass representations of the engines, tail rotor drive shaft, fuel, and soft mounted black boxes are generally sufficient; elastic-line representations for components such as the main rotor pylon/transmission, skid landing gear, and wings are sufficient; and beam-like tail booms must be modeled carefully at the higher frequencies.

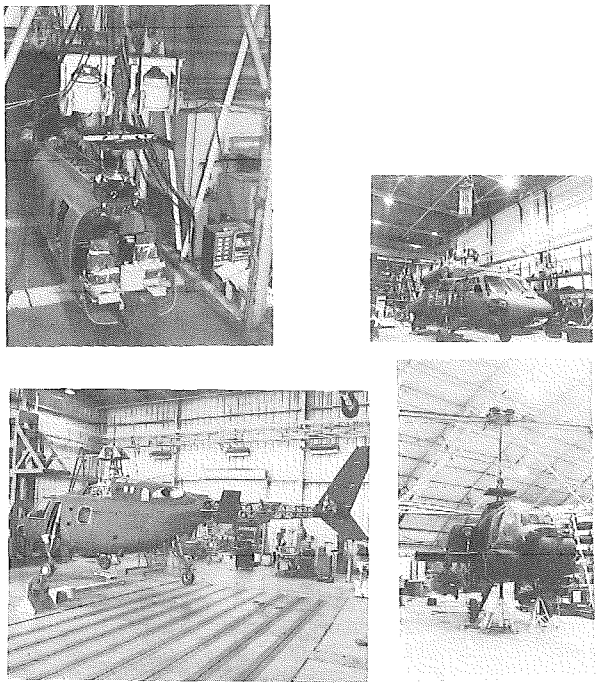

Figure 28. Ground vibration tests conducted.

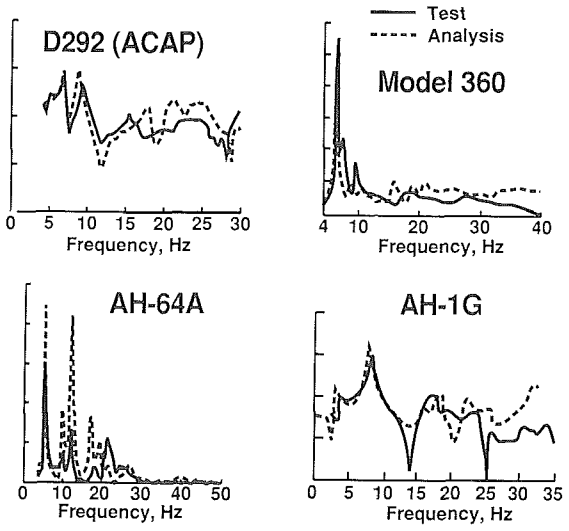

Figure 29. Typical test/analysis comparisons of airframe frequency response amplitudes.

Figure 30a.

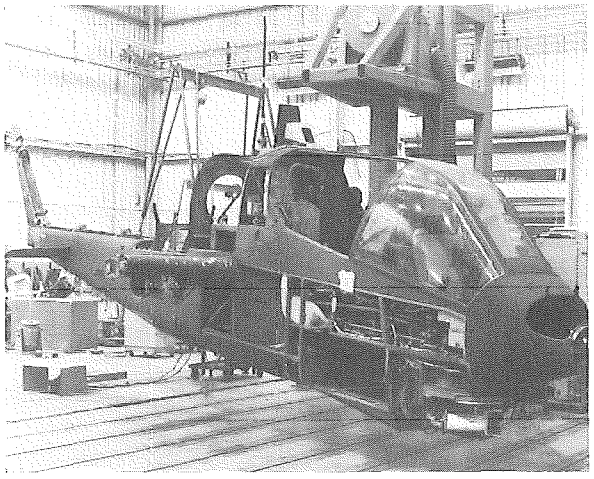

Figure 30b.

Figure 30. Difficult components study of AH-1G.

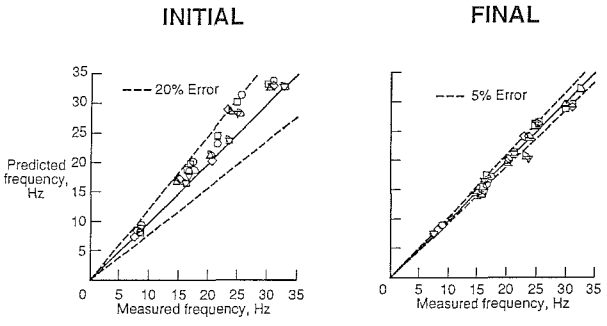

Figure 31. AH-1G natural frequency comparisons using initial and improved models.

Further results of the program are presented in ref. 22. The research conducted under this program has led to industry wide standards for modeling rotorcraft, improved modeling techniques, identified critical structural contributors

to airframe vibrations, and developed enhanced methods for performing ground vibration tests. Also defined were several key challenges which must be met for the industry to achieve the goal of producing a helicopter with a "jet smooth" ride.

Improvements to Tilt Rotor Performance Using Extension-Twist Coupling

Tiltrotor aircraft are designed to operate in both the helicopter and airplane flight modes. As depicted in Fig. 32, the twist that produces the minimum power requirement for hover is different from the twist that produces the minimum power requirement in forward flight. Typically the design twist is a compromise value between hover and forward flight requirements, giving optimum performance at neither condition. The author in ref. 23 proposes to take advantage of the difference in blade rotor speed between hover and forward flight to improve the performance at both conditions. This is accomplished by using aeroelastic tailoring with composite materials. The change in rotor speed produces a change in centrifugal force. The rotor speed in forward flight is typically 20 percent less than it is in hover. The blade is constructed of composites, designed to exhibit extension-twist coupling through the arrangement of off-axis ply angles and the stacking process. The change in centrifugal force supplies an extensive force which results in a change of tip twist due to the extension-twist coupling.

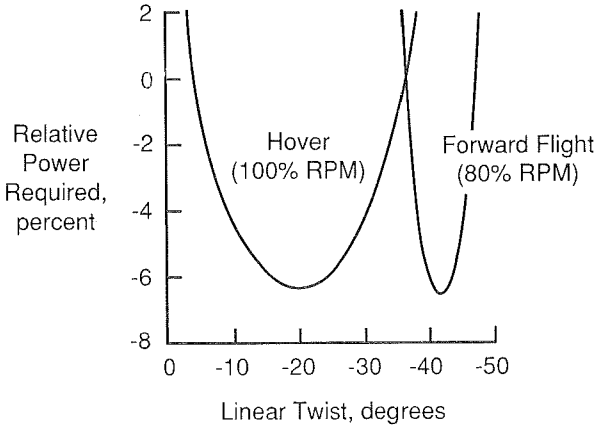

Figure 32. Relative power requirements versus twist for hover and forward flight.

As a first step in experimentally validating the extension-twist coupling concept a set of composite extension-twist coupled helicopter blades were designed and experimentally tested on a model in the TDT[24]. The blade spars were fabricated using graphite/epoxy composite material. The 0°/90° cloth weave was rotated off-axis to provide the extension-twist-coupled laminate. Two different mass distributions could be achieved by using ballast tubes within the spar that accepted tungsten ballast weights. A photograph of the blades on a model in the test section of the tunnel is shown in Fig. 33. The model was instrumented such that distributed twist angle could be measured as a function of blade RPM.

The change in blade elastic twist as a function of rotor speed is shown in Fig. 34. Test results showed maximum tip twist angle of 2.54 degrees for the unballasted configuration and 5.24 degrees for the ballasted blade. The results compared favorably with analytical results using a finite-element analysis. The blades were tested in hover at atmospheric pressure and in a near vacuum to determine the aerodynamic contributions to total twist. Although not shown, the results differed by a maximum of 0.17 degrees indicating that most of the twist is due to extension-twist coupling. This study has demonstrated the feasibility of using extension-twist-coupling to improve the performance of tilt rotor vehicles.

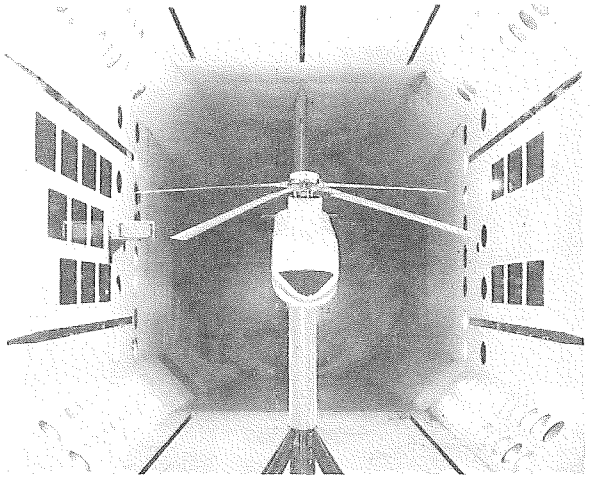

Figure 33. Extension-twist coupled rotor blades for helicopter model in TDT.

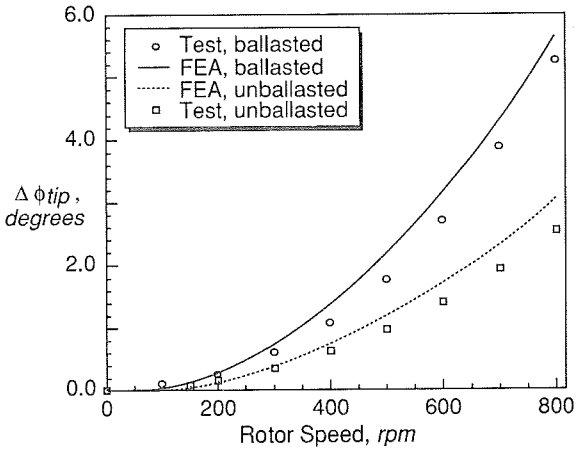

Figure 34. Change in blade elastic twist at tip as a function of rotor speed.

Concluding Remarks

Aeroelasticity and structural dynamics have been studied since the early days of manned flight. Indeed, aeroelastic and structural dynamic considerations are more important today than they have ever been.

This paper has presented the results of some recently completed research programs in aeroelasticity and structural dynamics at the NASA Langley Research Center. It has been shown that multifunctional active controls can be used

to control flutter and loads on future advanced fighter configurations. In an attempt to provide a well documented data base for validating unsteady aerodynamic codes a description and early results of an experimental program have been presented. It has been shown that the degradation in aeroelastic behavior due to thermal effects on a hypersonic vehicle can be offset by the use of active controls. The feasibility of using adaptive materials to control flutter has been demonstrated experimentally. A description of the latest unstructured grid methods for use in advanced computational unsteady aerodynamic codes has been presented. A review of a program to improve the ability of finite-element methods to predict rotorcraft vibrational characteristics has been described. Finally, the use of aeroelastic tailoring to improve the performance of tilt rotor vehicles has been described.

The results that have been presented indicate the wide range of aeroelasticity and structural dynamics research being conducted at the NASA Langley Research Center. NASA will continue to conduct research in this area in an effort to fully understand and predict associated phenomena to insure that future aircraft designs can fully exploit these technology advances.

Acknowledgment

The author wishes to acknowledge the work of the members of the Structural Dynamics Division at NASA Langley Research Center whose research is being overviewed in this paper.

References

1. Perry, B. III; Miller, G.D.; and Cole, S.R.: A Summary of the Active Flexible Wing Program. AIAA paper number 92-2080, presented at the 1992 AIAA Dynamic Specialist Meeting, Dallas, Texas, April 1992.
2. Reed, W.H. III; Foughner, J.T. Jr.; and Runyan, H.L. Jr.: Decoupler Pylon: A Simple, Effective Wing/Store Flutter Suppressor. Journal of Aircraft, Vol. 17, Number 3, March 1980.
3. Hoadley, S.T.; and McGraw, S.M.: The Multiple-Function Multi-Input/Multi-Output Digital Controller System for the AFW Wind-Tunnel Model. AIAA paper number 92-2083, presented at the 1992 AIAA Dynamic Specialist Meeting, Dallas, Texas, April 1992.
4. Batina, J.T.: Unsteady Transonic Algorithm Improvements for Realistic Aircraft Applications. AIAA Journal of Aircraft, Vol. 26, February 1989.
5. Silva, W.A.; and Bennett, R.M.: Further Investigations of the Aeroelastic Behavior of the AFW Wind-Tunnel Model Using Transonic Small Disturbance Theory. AIAA paper number 92-2082, presented at the 1992 AIAA Dynamic Specialist Meeting, Dallas, Texas, April 1992.
6. Mukhopadhyay, V.: Flutter Suppression Digital Control Law Design and Testing for the AFW Wind-Tunnel Model. AIAA paper number 92-2095, presented at the 1992 AIAA Dynamic Specialist Meeting, Dallas, Texas, April 1992.
7. Waszak, M.R.; and Srinathkumar, S.: Flutter Suppression for the Active Flexible Wing: Control System Design and Experimental Validation. AIAA paper number 92-2097, presented at the 1992 AIAA Dynamic Specialist Meeting, Dallas, Texas, April 1992.
8. Christhilf, D.M.; and Adams, W.M. Jr.: Multifunction Tests of a Frequency Domain Based Flutter Suppression System. AIAA paper number 92-2096, presented at the 1992 AIAA Dynamic Specialist Meeting, Dallas, Texas, April 1992.
9. Woods-Vedeler, J.A.; and Pototzky, A.S.: Rolling Maneuver Load Alleviation Using Active Controls. AIAA paper number 92-2099, presented at the 1992 AIAA Dynamic Specialist Meeting, Dallas, Texas, April 1992.
10. Moore, D.B.: Maneuver Load Control Using Optimized Feedforward Commands. AIAA paper number 92-2100, presented at the 1992 AIAA Dynamic Specialist Meeting, Dallas, Texas, April 1992.
11. Bennett, R.M.; Eckstrom, C.V.; Rivera, J.A.; Dansberry, B.E.; Farmer, M.G.; and Durham, M.H.: The Benchmark Aeroelastic Models Program-Description and Highlights of Initial Results. Presented at the AGARD Structures and Materials Panel Specialists' Meeting on Transonic Unsteady Aerodynamics and Aeroelasticity, San Diego, California, October 1991.
12. Farmer, M.G.: A Two-Degree-of-Freedom Flutter Mount System with Low Damping for Testing Rigid Wings at Different Angles of Attack. NASA TM-83302, 1982.
13. Rivera, J.A.; Dansberry, B.E.; Bennett, R.M.; Durham, M.H.; and Silva, W.A.: NACA 0012 Benchmark Model Experimental Flutter Results with Unsteady Pressure Distributions. AIAA paper number 92-2396, presented at the AIAA/ASME/ASCE/AHS/ASC 33rd Structures, Structural Dynamics and Materials Conference, Dallas, Texas, April 1992.
14. Heeg, J.; Gilbert, M.G.; and Pototzky, A.: Active Control of Aerothermoelastic Effects for a Conceptual Hypersonic Aircraft. Paper presented at the AIAA Guidance, Navigation, and Controls Conference, Portland, Oregon, August 1990.
15. Ehlers, S.M.: Aeroelastic Behavior of an Adaptive Lifting Surface. PhD Dissertation, Purdue University, 1991.
16. Lazarus, K.B.; Crawley, E.F.; and Lin, C.Y.: Fundamental Mechanisms of Aeroelastic Control with Control Surface and Strain Actuation. Proceedings of the AIAA/ASME/ASCE/AHS/ASC 32nd Structures, Structural Dynamics and Materials Conference, Baltimore, Maryland, April 1991.
17. Scott, R.C.: Control of Flutter Using Adaptive Materials. MS Thesis, Purdue University, May 1990.
18. Heeg, J.: An Analytical and Experimental Investigation of Flutter Suppression via Piezoelectric Actuation. AIAA paper number 92-2106, presented at the 1992 AIAA Dynamic Specialist Meeting, Dallas, Texas, April 1992.
19. Edwards, J.W.; and Malone, J.B.: Current Status of Computational Methods for Transonic Unsteady Aerodynamic and Aeroelastic Applications. Presented at the AGARD Structures and Materials Specialists' Meeting on Transonic Unsteady Aerodynamics and Aeroelasticity, San Diego, California, October 1991.

20. Batina, J.T.: Unsteady Euler Algorithm with Unstructured Dynamic Mesh for Complex-Aircraft Aeroelastic Analysis. AIAA Journal, Vol. 29, No. 3, March 1991.

21. Rausch, R.D.; Batina, J.T.; and Yang, H.T.Y.: Spatial Adaption Procedures on Unstructured Meshes for Accurate Unsteady Aerodynamic Flow Computation. AIAA Paper No. 91-1106, April 1991.

22. Kvaternik, R.G.: The NASA/Industry Design Analysis Methods for Vibrations (DAMVIBS) Program—Accomplishments and Contributions. Presented at the AHS National Technical Specialists' Meeting on Rotorcraft Structures, Williamsburg, Virginia, October 1991.

23. Nixon, M.W.: Improvements to Tilt Rotor Performance Through Passive Blade Twist Control. NASA TM-1000583, AVSCOM TM-88-B-010, April 1988.

24. Lake, R.C.; Nixon, M.W.; Wilbur, M.L.; Singleton, J.D.; and Mirick, P.H.: A Demonstration of Passive Blade Twist Control using Extension-Twist Coupling. AIAA paper number 92-2468, presented at the 33rd Structures, Structural Dynamics and Materials Conference, Dallas, Texas, April 1992.